PCCP

Accepted Manuscript

ROYAL SOCIETY OF CHEMISTRY

www.rsc.org/pccp

PCCP

RSCPublishing

ARTICLE

Synergetic effect in Ir-Au/TiO_2 catalysts in the total oxidation of propene: Influence of the activation conditions.

Cite this: DOI: 10.1039/xoxxoooooox

Received ooth January 2015,
Accepted ooth January 2015

DOI: 10.1039/xoxxoooooox

www.rsc.org/

Antonio Aguilar-Tapia[a], Rodolfo Zanella[a*], Christophe Calers[b,c], Catherine Louis[b,c] and Laurent Delannoy[b,c]

Iridium was added to the Au/TiO_2 system to try to enhance its catalytic activity in the reaction of propene oxidation, performed in conditions close to those used in the studies of decomposition of Volatile Organic Compounds (1200 ppm propene and 9 vol% O_2 in He). Titania supported Ir-Au (Ir/Au = 1) was prepared by sequential deposition-precipitation with urea (DPU) of Ir then Au. The effect of the activation conditions (hydrogen or air at 400 °C) was investigated. The study of the activation conditions of Ir-Au/TiO_2 showed that activation under hydrogen at 400 °C generated a catalyst more active than the monometallic ones, while Ir-Au/TiO_2 activated in air remained as poorly active as Au/TiO_2. TEM characterization showed the formation of metallic particles of similar size (2-3 nm) in both monometallic Au/TiO_2 and bimetallic Ir-Au/TIO_2. Characterizations especially by DRIFTS using CO as a probe molecule, suggest the presence of Ir-Au interaction, IrO_2-Au^0 interaction when the sample is calcined and Ir^0-Au^0 bimetallic particles when it is reduced. XPS and TPR characterizations showed that gold hinders to some extent the reoxidation of iridium in reduced bimetallic Ir-Au/TiO_2 catalyst. The enhanced catalytic activity of the reduced bimetallic Ir-Au/TiO_2 catalyst is attributed to a surface Ir^0-Au^0 synergism.

1. Introduction

Low temperature catalytic oxidation of volatile organic compounds (VOC) has been widely studied over nano-sized gold particles supported on a wide variety of metal oxides, such as CeO_2, FeO_2, TiO_2, ZrO_2, and tested with different molecules like toluene, benzene, n-hexane, propane, propene, methanol highly diluted in air or oxygen.[1–7]

In a previous work, Delannoy et al.[8] studied the effect of the support on gold catalysts in the reaction of propene oxidation; they showed that Au supported on CeO_2 was a very active catalyst, as CeO_2 brings its properties of lattice oxygen mobility and oxygen storage capacity, whereas Au supported on TiO_2 had a lower activity.

a Centro de Ciencias Aplicadas y Desarrollo Tecnológico (CCADET), Universidad Nacional Autónoma de México (UNAM), México D. F., México A. P. 70-186

b Sorbonne Universités, UPMC Univ Paris 06, UMR 7197, Laboratoire de Réactivité de Surface, 4 Place Jussieu, F-75005, Paris, France

c CNRS, UMR 7197, Laboratoire de Réactivité de Surface, 4 Place Jussieu, F-75005, Paris, France

It has been shown previously that the addition of an iridium component (Ir/La_2O_3) to Au/Fe_2O_3 catalyst enhanced the catalytic activity of gold catalyst activated by calcination, for the decomposition of dioxins at temperatures below 473 K.[9] To determine the structure of the catalyst, the authors studied by HRTEM a model catalyst obtained by simultaneous deposition of gold and iridium on a rutile single crystal.[10] The HRTEM images revealed that the gold particles were deposited on the top of IrO_2 pillars that were in direct contact with the support. The authors claimed that the crystalline IrO_2 pillars resulted for the calcination of the Au-Ir complex formed during co-deposition. Density functional theory calculations performed by Liu et al.[11] with the Au/IrO_2-TiO_2 system showed that the presence of iridium oxide favored the formation of Au/IrO_2 interface with respect to that of Au/TiO_2, which was found to be more active in CO oxidation and to hinder the sintering of gold particles during the reaction.

More recently Gómez-Cortés et al.[12] showed that sequential deposition-precipitation of iridium first on TiO_2 followed by calcination under air, then deposition of Au is a better method than co-deposition-precipitation, and that activation under H_2 generates a more active Au-Ir/TiO_2 catalyst in CO oxidation than calcination. Rietveld refinement and micro EDS

characterization[13] showed that the metal particles in reduced Au-Ir/TiO_2 were mostly bimetallic Au-Ir despite the fact that gold and iridium are practically immiscible in the bulk,[14] with also the presence of both monometallic Au and Ir particles, and that the bimetallic particles were responsible for the higher stability and catalytic activity in the oxidation of CO compared to Au/TiO_2.

Based on all these previous works, we decided to investigate the effect of iridium addition to the Au/TiO_2 system in the reaction of propene oxidation, for which the titania supported gold catalyst has only a poor activity. The reaction was performed in condition of low concentration of propene and large excess of oxygen, so as to mimic the conditions of catalytic decomposition of a volatile organic compound of hydrocarbon-type. The influence of the activation conditions were also investigated, since depending on the kind of thermal pretreatment, under air (calcination) or H_2 (reduction), different species could be expected, and have an influence in the catalytic properties. Actually, in the case of the monometallic catalysts, it is known that supported gold precursor thermally decomposes in air to form Au^0,[15] hence Au^0 is expected after reduction or calcination. For supported Ir, activation under air leads to IrO_2[12,16,17] species while a reduction under H_2 to Ir^0.

2. Experimental.

2.1 Catalysts preparation

Titania Evonik P25 was used as support (45 m^2 g^{-1}, nonporous, 70% anatase, 30% rutile, purity >99.5%). Commercial $HAuCl_4 \cdot 3H_2O$ and $IrCl_4 \cdot 4H_2O$, both from Aldrich, were used as gold and iridium precursors. Before preparation, TiO_2 was dried in air at 100 °C for at least 24 h.

2.1.1 Preparation of monometallic samples

The preparation of the 3 wt% Au/TiO_2 or Ir/TiO_2 sample was performed by deposition-precipitation with urea (DPU) in the absence of light, following previously reported procedure.[18–20] Briefly, the gold precursor, $HAuCl_4$ (4.2 x 10^{-3} M) or iridium precursor $IrCl_4$ (4.2 x 10^{-3} M) and urea (0.42 M) were dissolved in 50 mL of distilled water. Then, 1 g of titania was added to this solution. Thereafter, the suspension temperature was increased to 80 °C and kept constant 16 h under stirring.

After deposition-precipitation, the samples were washed with water and centrifuged four times, and dried under vacuum for 2 h at 80 °C. After drying, the samples were stored at room temperature in a desiccator under vacuum, away from light in order to prevent any alteration.[20] These conditions should allow to reach Au and Ir loadings of 3 wt%, i.e., the equivalent of 0.4 at.% for both elements. Note that the molecular masses of Ir (192.22 g mol^{-1}) and Au (196.96 g mol^{-1}) are almost the same.

2.1.2 Preparation of bimetallic samples

A sequential deposition method was used to prepare the bimetallic catalyst Ir-Au (3 wt% - 3 wt%). Iridium was first deposited on TiO_2 by deposition-precipitation with urea as described above. After drying at 80 °C for 2 h, the Ir/TiO_2 sample was calcined in air at 500 °C for 2 h at a heating rate of 2 °C min^{-1}, before gold was deposited by deposition-precipitation. The same procedure of washing and drying as above was applied.

2.2 Catalytic activity

The reaction of propene oxidation was carried out in a microreactor in pyrex. It is important to note that since the atomic mass of Ir and Au is almost the same, there are twice as much of metal atoms in the bimetallic than the monometallic catalysts (Table 1). As a consequence, a mass of 150 mg was employed for the monometallic supported Au and Ir catalysts while the mass of the bimetallic Ir-Au catalyst used was only 75 mg to which 75 mg of TiO_2 was added to ensure a constant number of metal atoms in the catalytic bed and the same space velocity as for the monometallic catalysts.

The catalysts were activated *in situ* under extra dry synthetic air (calcination) or ultra-high purity H_2 (reduction) (100 mL min^{-1}) from RT to 400 °C (2 °C min^{-1}) with a 2 h plateau at the final temperature, this temperature arises from a series of tests performed with the bimetallic sample activated under H_2 at different temperatures, which showed that activation at 400 °C resulted in the most active catalysts for this reaction (results not shown). The catalysts were cooled down to RT under the same gas, and the reaction mixture consisting of 1200 ppm C_3H_6 and 9 vol.% O_2 in He was introduced with a flow rate of 150 mL min^{-1} which corresponds to a GHSV = 7800 h^{-1}. The reaction temperature was increased stepwise from room temperature to the temperature corresponding to 100 % of conversion (i.e. up to a maximum of 325 °C) at a heating rate of 1 °C min^{-1}. The heating rate was intentionally slow to perform the test at quasi-steady state. C_3H_6 consumption and CO_2 production were monitored using a Varian Micro GC QUAD CP4900 equipped with two analysis channels (Molsieve 5A for O_2 and CO detection and Poraplot Q for CO_2 and C_3H_6 detection)

2.3 Characterization techniques

Chemical analysis of Au and Ir in the samples to determine the actual loadings was performed by X-ray fluorescence (XRF) using a spectrometer XEPOS HE (AMETEK). The Au and Ir weight loadings were expressed in grams of each metal per gram of sample.

After *ex situ* thermal treatment under the same conditions as for the C_3H_6 oxidation reaction, the samples were examined by transmission electron microscopy in a Jeol-2010 FasTem analytical microscope equipped with a Z-contrast annular detector. The average size of particles and the histograms of particles sizes were established from the measurement of 800 to 1000 particles. The size limit for the detection of the metal particles on TiO_2 was about 0.6 nm. The average particle diameter d_s was calculated with the formula: $d_s = \sum n_i d_i / \sum n_i$ where n_i is the number of particles of diameter d_i. The standard

Table 1 Theoretical and experimental Au and Ir loadings in the studied catalysts.

Catalyst	Metal loading, wt%				Experimental Au/Ir atomic ratio
	Nominal Ir loading	Experimental Ir loading	Nominal Au loading	Experimental Au loading	
Au/TiO_2	-	-	3	3	-
Ir/TiO_2	3	2.9	-	-	-
$Ir\text{-}Au/TiO_2$	4.2	2.7	3	2.8	1:1

deviation was calculated with the formula: $\sigma = [\sum(d_i - d_s)^2 / \sum n_i]^{1/2}$.

Diffuse reflectance UV-Visible spectra of the catalysts were obtained using a CARY5000 spectrophotometer equipped with a Praying Mantis and a high temperature reaction chamber (Harrick).

The spectra were recorded from 300 to 800 nm during thermal treatment under hydrogen. In each experiment, approximately 25 mg of dried sample was packed in the sample holder and pretreated *in situ* under hydrogen flow (30 mL min^{-1} and 2 °C min^{-1}) up to 400 °C, followed by a 30-min-plateau. A spectrum of Teflon (from Aldrich) was used as reference.

The hydrogen temperature programmed reduction (H_2-TPR) study of the dried catalysts was performed in a Micromeritics-Autochem 2910 unit under a flow of 5% H_2/Ar gas mixture (25 mL min^{-1}) and with a heating rate of 7.5 °C min^{-1}, from room temperature to 900 °C. H_2O produced during the reduction process was trapped before the TCD detector.

XPS spectra were collected on an Omicron (ESCA+) X-ray photoelectron spectrometer, using an Al Kα (hν = 1486.6 eV) X-ray source powered at 14kV and 20mA. After collection, the binding energies were calibrated with respect to the C–C/C–H components of the C 1s peak (binding energy = 284.8 eV). Spectra processing was carried out using the Casa XPS software package.

CO adsorption was followed by DRIFT spectroscopy to characterize the metallic surface. The experiments were carried out in a Nicolet 670FT-IR spectrophotometer equipped with a Praying Mantis and a low/high temperature reaction chamber by Harrick. In each experiment, approximately 40 mg of dried sample was packed in the sample holder and pretreated *in situ* in hydrogen or air flow (40 mL min^{-1}, heating rate 2 °C min^{-1}) up to 400 °C followed by a plateau for 1 h. After thermal treatment, the sample was cooled down to room temperature (RT) under the same gas flow and then purged with N_2 before the introduction of 5% CO in N_2 (40 mL min^{-1}). A spectrum recorded under N_2 was used as reference and then a spectrum was recorded after 5 min under CO flow.

3. Results

3.1 Elemental analysis

Let us remind that the nominal metal loadings of the monometallic catalysts were 3 wt% for Au and Ir, which corresponds to 0.4 at.% for both samples. Table 1 compares the nominal and the measured gold and iridium loadings in wt% and the Au/Ir atomic ratio for the Ir-Au sample. As expected from former studies on gold catalysts,[18,21,22] the experimental gold loadings are very close to the theoretical value (3 wt%) whether the catalyst is mono or bimetallic. In the case of Ir/TiO_2, almost all the iridium was deposited on TiO_2 (2.9 wt%), which confirms that Ir can be deposited by the method of deposition-precipitation with urea.[13,23]

However the experimental Ir loading in the bimetallic sample was lower than the nominal loading, probably because of iridium leaching during Au deposition. As a consequence, we had to increase the nominal Ir loading to 4.2 wt% to obtain an Ir one close to 3 wt% and an Au:Ir atomic ratio close to 1 (Table 1).

3.2 Size of the nanoparticles after activation

Fig. 1 shows typical HAADF images of Au/TiO_2, Ir/TiO_2 and $Ir\text{-}Au/TiO_2$ activated at 400 °C under H_2 or air, and Table 2 reports the corresponding average metal particle sizes. The average particle sizes of the reduced samples were slightly smaller than those of the calcined ones. For Au/TiO_2 the average size was 2.1 nm after reduction and 3.2 nm after calcination; for bimetallic $Ir\text{-}Au/TiO_2$ catalyst, the average size was 2.3 nm after reduction and 2.9 after calcination, for Ir/TiO_2 catalyst the particles were smaller, 1.3 nm after reduction and 1.7 nm after calcination. It is worth to note that there is no big difference between the average particle size of the reduced Au/TiO_2 and $Ir\text{-}Au/TiO_2$ catalysts, but both are larger than the one of Ir/TiO_2.

Note that the lattice parameters of gold and iridium are very similar, so it has not been possible to establish the bimetallic character of the particles in the $Ir\text{-}Au/TiO_2$ catalyst by HRTEM.

Table 2 Average metal particle size determined by TEM in the catalysts activated in H_2 or air at 400 °C.

Catalyst	Activated in hydrogen		Activated in air	
	Average particle size (nm)	Standard deviation (nm)	Average particle size (nm)	Standard deviation (nm)
Au/TiO_2	2.1	0.68	3.6	1.19
$IrAu/TiO_2$	2.3	0.68	2.9	1.04
Ir/TiO_2	1.3	0.32	1.7	0.48

3.3 Reducibility of gold and iridium in as-prepared samples

3.3.1 TPR characterization

The reducibility of the as-prepared samples was studied by TPR. As a reference, the TPR profile of TiO_2 (Fig. 2A) does not show any appreciable peaks associated to the reduction of

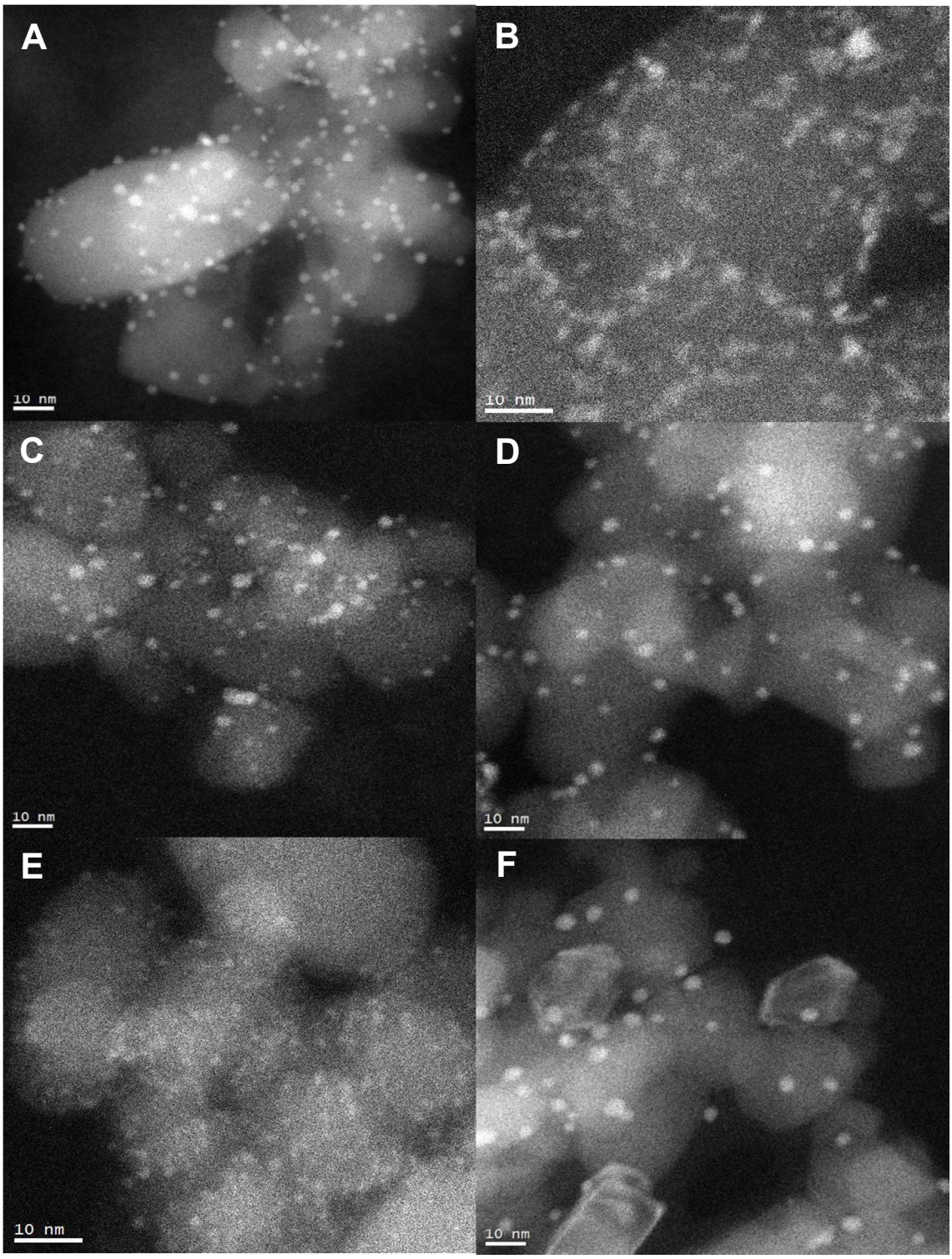

Fig. 1 HAADF images of Au/TiO_2 (A) reduced and (B) calcined, Ir/TiO_2 (C) reduced and (D) calcined and $Ir\text{-}Au/TiO_2$ (E) reduced and F) calcined.

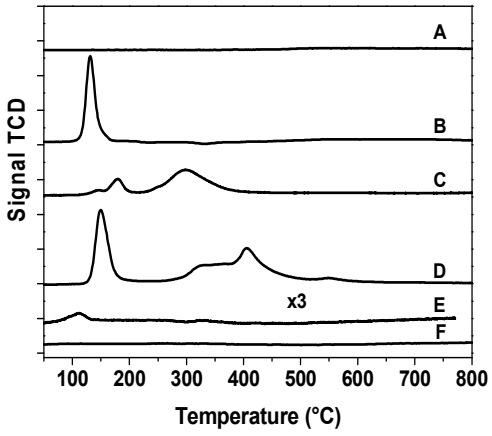

Fig. 2 TPR profiles of (A) TiO_2 support, (B) Au/TiO_2, (C) Ir/TiO_2 calcined at 500 °C, (D) Ir-Au/TiO_2, (E) Ir/TiO_2 exposed to air for one week after TPR test and (F) Ir-Au/TiO_2 exposed to air for one week after TPR test.

Ti species. The reduction profile of Au/TiO_2 (Fig. 2B) appears as a single peak between 100 and 170 °C with a maximum at 130 °C; this reduction peak has been assigned to the reduction of Au^{III} precursor formed during the DP urea process.[24,25] Three peaks are present in the TPR profile of Ir/TiO_2 calcined at 500 °C (Fig. 2C), at about 145, 180 and 300 °C. The weaker peaks at 145 and 180 °C can be assigned to the reduction of large iridium oxide particles, whereas the peak at 300 °C can be attributed to iridium oxide species with higher interaction with the support.[23,26] The TPR profile of Ir-Au/TiO_2 (Fig. 2D) shows a shift of all the reduction peaks towards higher temperature compared to the ones of the monometallic samples: the reduction of gold occurs now at 150 °C, and the reduction of iridium appears as a broad peak between 270 and 510 °C.

After TPR (up to 800 °C), the Ir/TiO_2 and Ir-Au/TiO_2 samples were exposed to air for one week at ambient conditions and submitted to a second TPR so as to detect a possible reoxidation of the metallic species.

A very small hydrogen consumption peak is observed between 70 and 140 °C for the Ir/TiO_2 sample (Fig. 2E), indicating surface reoxidation of iridium particles during air contact; this is not observed with the bimetallic Ir-Au sample (Fig. 2F).

3.3.2 UV-Visible characterization

The UV-Visible spectra of the as-prepared Au/TiO_2, Ir/TiO_2, and Ir-Au/TiO_2 samples were recorded during *in situ* reduction under hydrogen at increasing temperature between RT and 400 °C (Fig. 3). The monometallic Au sample (Fig. 3A) develops a broad band between 400 and 800 nm that increases in intensity as reduction temperature increases. The band centered at ~542 nm is associated to the surface plasmon resonance (SPR) of metallic gold;[27–29] the color of the sample changed from yellow at RT to violet after treatment above 135 °C, confirming the reduction of gold observed by TPR. In the case of the monometallic Ir/TiO_2 sample (Fig. 3B), there is an increase of the absorbance in the visible region that can be associated to the change of color of the sample from beige at RT to a dark grey, indicating the reduction of iridium during the treatment as already observed during Ir colloid preparation.[30,31] For the bimetallic Ir-Au/TiO_2 sample (Fig. 3C) the plasmon band of Au^0 is visible with a maximum at ~533 nm and its intensity increases with temperature while the color change from strong dark grey at RT (due to the color of calcined Ir/TiO_2, see section 2.1.2) to violet above 150 °C, indicating the reduction of gold in the sample.

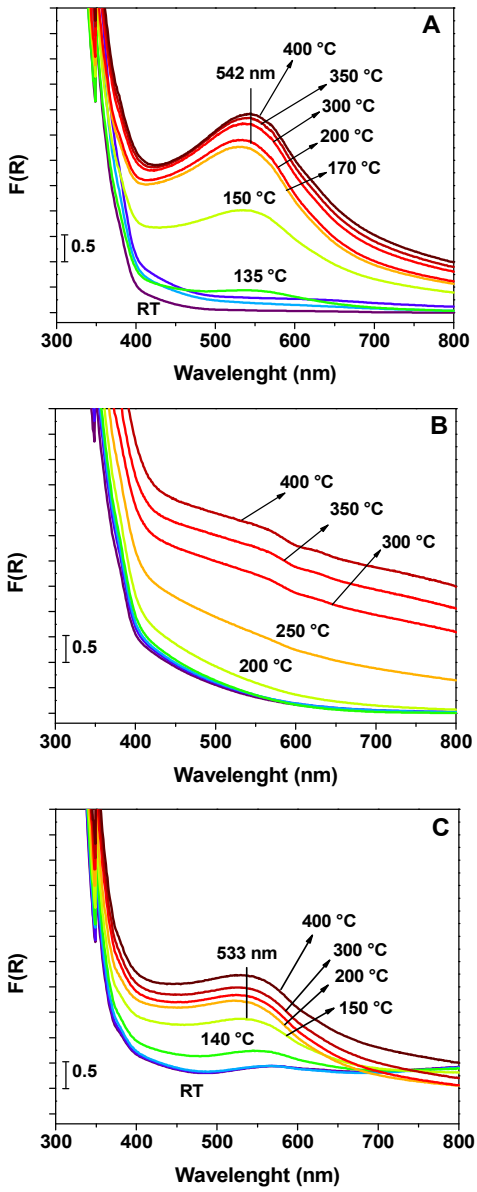

Fig. 3 UV-Visible spectra of samples reduced *in situ* under hydrogen at increasing temperatures for as-prepared (A) Au/TiO_2, (B) Ir/TiO_2 and (C) Ir-Au/TiO_2 samples

It is known that the plasmon band shape and position are dependent on particle size, shape and surrounding environment.[32–35] Since the metal particles in Au/TiO_2 and Ir-Au/TiO_2 samples have almost the same size (Table 2), the shift in the position of the SPR band of the Ir-Au sample (Fig. 3C) and the attenuation of its intensity, compared to that of the Au sample, could be due to the presence of Ir and its interaction with gold in the particles.

3.4 Propene oxidation

3.4.1 Influence of the activation treatment

Fig. 4 reports the comparison of the propene conversion as a function of the reaction temperature of monometallic Au/TiO_2 and Ir/TiO_2 and bimetallic Ir-Au/TiO_2 activated at 400 °C under air (Fig. 4A) or H_2 (Fig. 4B).

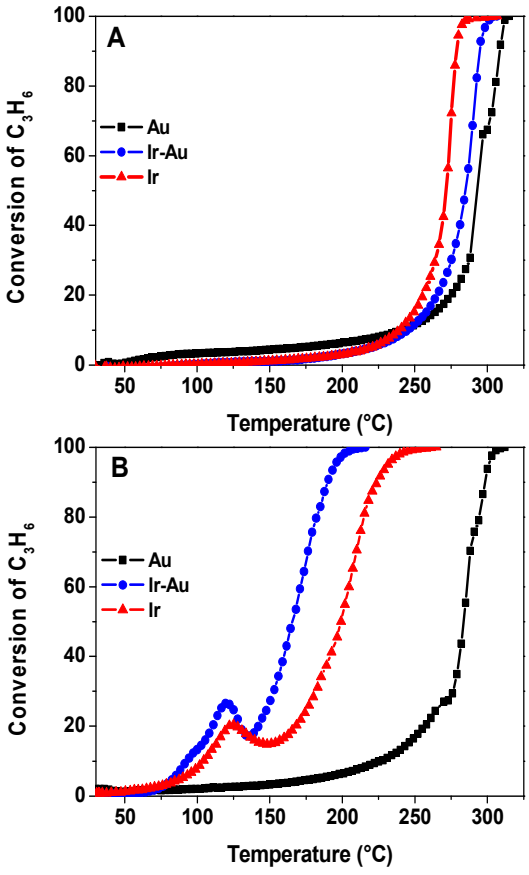

Fig. 4 Propene oxidation light-off curves of monometallic Au/TiO_2 (square) and Ir/TiO_2 (triangle) and bimetallic Au-Ir/TiO_2 (circle) catalysts activated at 400 °C (A) under air (B) under H_2.

Let us remind that the total number of metal atoms in the catalytic bed was maintained constant by diluting the bimetallic Ir-Au/TiO_2 catalyst with bare TiO_2 (see section 2.2) and the bare TiO_2 support does not show any activity between RT and 500 °C.[8] Note also that for all the catalysts and whatever the reaction temperature, the propene is fully converted into CO_2 and H_2O with no detectable trace of CO. Fig. 4A shows that all of the calcined samples are poorly active below 250 °C, and the bimetallic catalyst shows an activity with a $T_{50\%}$ (temperature corresponding to 50% conversion of propene) of 285 °C, which is intermediate between the $T_{50\%}$ of the two monometallic catalysts (270 °C for Ir/TiO_2 and 295°C for Au/TiO_2).

In contrast, when the samples are activated under H_2 (Fig. 4B), the Ir/TiO_2 and Ir-Au/TiO_2 catalysts show a strong increase in catalytic activity compared to the calcined samples while the activity of gold remains almost unchanged ($T_{50\%}$ = 285 °C). Both Ir/TiO_2 and Ir-Au/TiO_2 start to be active below 100 °C with a hump of conversion (~20%) around 120 °C. Then Ir-Au/TiO_2 clearly exhibits a higher activity ($T_{50\%}$ = 165 °C) than monometallic Ir/TiO_2 ($T_{50\%}$ = 200 °C) and *a fortiori* than Au/TiO_2, which means that the bimetallic Ir-Au sample shows a synergetic effect. Hence, the nature of the gas of activation is much more significant for monometallic Ir/TiO_2 and bimetallic Ir-Au/TiO_2 catalysts than for Au/TiO_2, the thermal treatment under H_2 produces more active Ir-based catalysts in the reaction of propene oxidation, and the addition of Ir to Au/TiO_2 catalyst enhances it activity provided that the catalyst is activated under H_2.

In order to observe some possible changes in the catalytic behavior of the samples after a first run in propene oxidation, the Ir-Au/TiO_2 (Fig. 5A) and Ir/TiO_2 (Fig. 5B) catalysts were submitted to a second catalytic test (after cooling down to RT under the reaction mixture). These experiments show that in the second reaction run, the hump of activity at temperature below 150 °C has disappeared and that the catalyst shows a slight decrease in activity at temperature above 150 °C, which is more pronounced for the monometallic Ir/TiO_2 catalyst.

The samples activated under hydrogen were submitted to $C_3H_6 + O_2$ stream for 24 h in order to determine their stability (see supporting information). Fig. 1S shows that all the samples were stable during the period of the test.

3.5 XPS results

XPS measurements were performed in order to determine the evolution of the oxidation state of gold and iridium in mono and bimetallic samples during the reaction of propene oxidation. Fig. 6 and 7 show the XPS spectra of the Ir 4f core level of Ir/TiO_2 and Ir 4f and Au 4f core levels of Ir-Au/TiO_2 respectively, after *ex situ* reduction, during propene oxidation up to 150 °C (after the hump of activity) and after reaction up to 250 °C, i.e., after the catalysts have reached 100% conversion of propene; note that a contribution of Ti 3s at ~62 eV from the support appears in the Ir 4f region. Table 3 summarizes the observed binding energies of the studied catalysts. It is worth to note that before characterization by XPS, the samples were exposed to air during the transfer in the XPS equipment; hence surface reoxidation could have occurred.

Figs. 7 D, E and F shows that the Au $4f_{7/2}$ core level of the Ir-Au sample remains unchanged after *ex situ* activation (83.6 eV),

Table 3. Binding energies and relative surfaces of the XPS Ir $4f_{7/2}$ and Au $4f_{7/2}$ peaks of Ir/TiO_2 and $Ir\text{-}Au/TiO_2$ after ex situ activation and after different stages of the reaction of propene oxidation; transfer to XPS was performed in air

Sample	Treatment	Ir^0		Ir^{4+}		Au^0	
		BE (eV)	%	BE (eV)	%	BE (eV)	%
Ir	H_2/400°C *	60.5	64	61.8	36	--	--
	Reaction up to 150 °C	60.5	20	61.7	80	--	--
	Reaction up to 250 °C	--	0	61.9	100	--	--
Ir-Au	H_2/400°C *	60.3	70	62.1	30	83.6	100
	Reaction up to 150 °C	60.3	68	62.2	32	83.4	100
	Reaction up to 250 °C	60.3	42	61.4	58	83.3	100

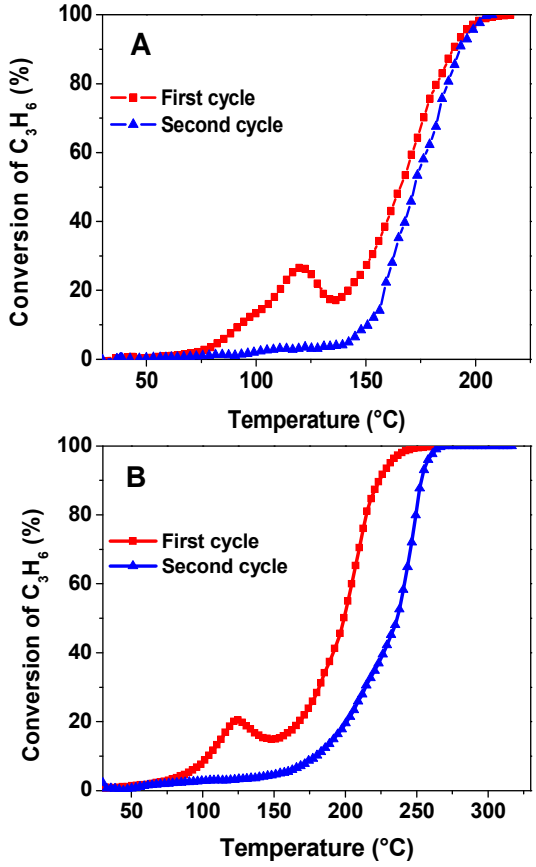

Fig. 5 Propene oxidation light-off curve of bimetallic $Ir\text{-}Au/TiO_2$ (A) and Ir/TiO_2 (B) catalysts activated at 400 °C under H_2 (square) followed by a second reaction run (triangle).

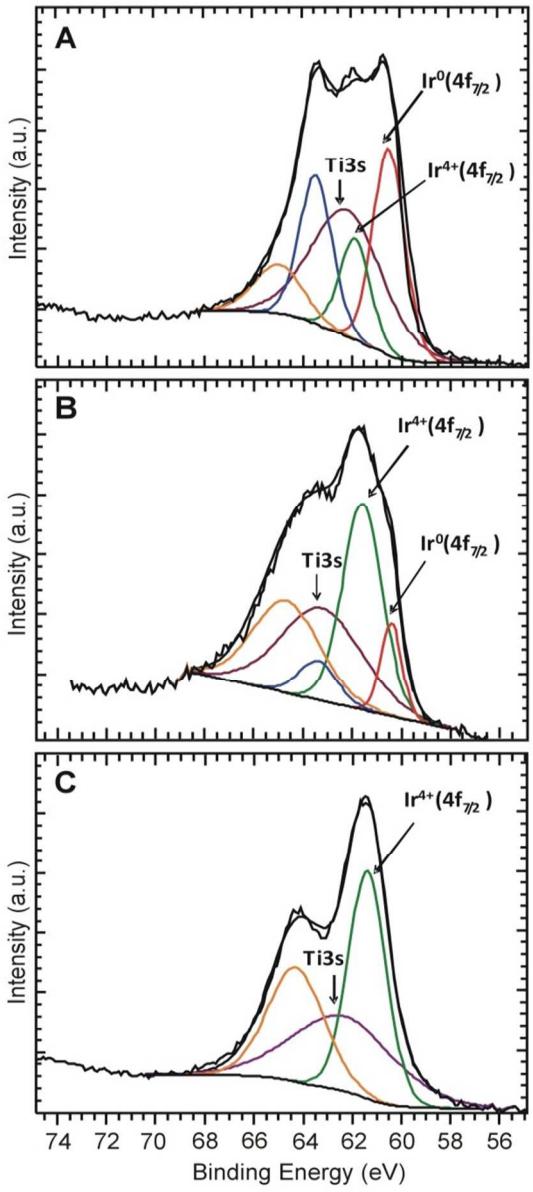

Fig. 6 XPS spectra of as-prepared Ir/TiO_2 after (A) *ex situ* activation under H_2, (B) after propene oxidation reaction up to 150 °C and (C) up to 250 °C at 100% conversion.

up to 800 °C, and it is possible that activation under after reaction up to 150°C (83.4 eV) or up to 250°C (83.3 eV), and correspond to Au^0,[1,8,36,37] indicating that gold remains completely reduced at all of the stages of the reaction.

After *ex situ* reduction at 400 °C, the monometallic Ir/TiO_2 sample (Fig. 6A) exhibits an Ir $4f_{7/2}$ peak at 60.5 eV corresponding to Ir^0 (64%)[38,39] and another one at 61.8 eV assigned to Ir^{4+} (36%).[40] The spectrum of the reduced bimetallic Ir-Au sample (Fig. 7A) shows a major contribution corresponding to Ir^0 at 60.3 eV (70%) and a minor one related to Ir^{4+} at 62.1 eV (30%). It can be anticipated that the contribution of the oxidized iridium (36%, Table 3) in both

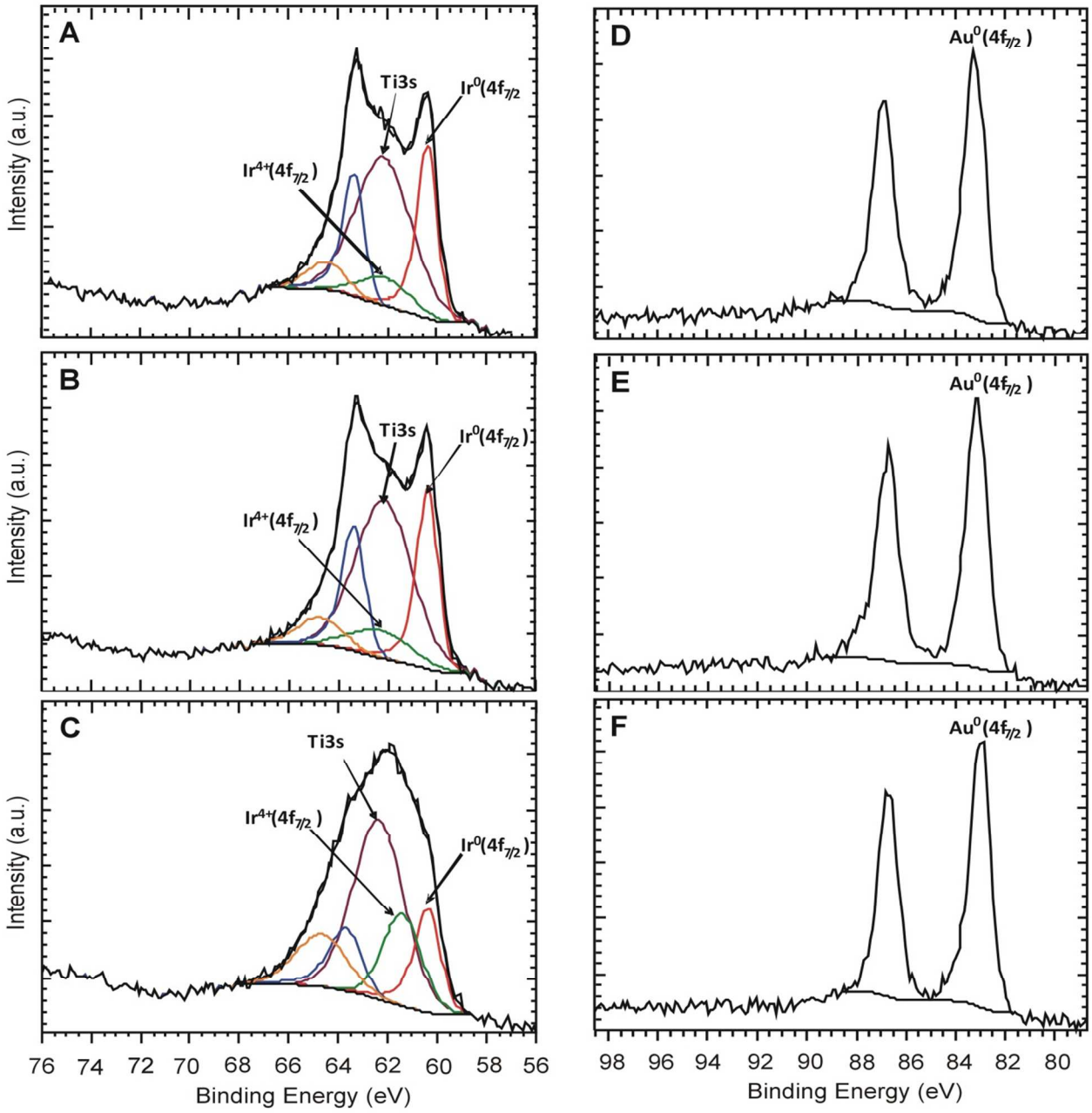

Fig. 7 XPS spectra of Ir-Au/TiO_2 at the Ir(4f) core level (A) after *ex situ* activation under H_2 at 400 °C, (B) after propene oxidation reaction up to 150 °C and (C) after 100% conversion of propene oxidation and at the Au(4f) core level (D) after *ex situ* activation under H_2 at 400 °C, (E) after propene oxidation reaction up to 150 °C and (F) up to 250 °C at 100% conversion.

samples result from a reoxidation of the particles during air transfer. According to TPR, the Ir^0 particles in Ir/TiO_2 are superficially reoxidized in air (Fig. 2E); this was not observed for $Ir\text{-}Au/TiO_2$ (Fig. 2F), but it must be underlined that these TPR experiments were performed after a first TPR performed H_2 at 400 °C generated smaller particles, more sensitive towards reoxidation during contact with air. At this stage, it can be considered that Ir is completely reduced after reduction at 400 °C for 2 h, whatever the sample. For the monometallic Ir/TiO_2 sample (Fig. 6B), the contribution of the oxidized iridium (Ir^{4+} 80%) has increased drastically (Table 3) whereas for the $Ir\text{-}Au/TiO_2$ sample (Fig. 7B and Table 3), the metallic iridium contribution remained the main one (Ir^0 68%).

The spectra were also recorded after propene oxidation reaction up to 150 °C, i.e., after the hump of activity at ~120 °C (Fig. 4B), and large differences were observed between the two samples even considering that some oxidation may have happened during air transfer.

After propene oxidation reaction up to 250 °C, the Ir/TiO_2 sample shows a single Ir $4f_{7/2}$ contribution at 61.9 eV indicating that iridium is completely oxidized at the end of the reaction (Fig. 6C and Table 3) whereas, there is still a large amount of metallic iridium (Ir^0 42%) in the bimetallic sample, as shown in Fig. 7C and Table 3.

3.6 Surface composition of the catalysts by CO-DRIFTS

To investigate the surface composition of the particles, CO adsorption on Ir-Au catalyst was studied by DRIFTS after *in situ* activation under hydrogen or air at 400 °C and compared with the monometallic Au and Ir samples.

Fig. 8A compares the DRIFT spectra recorded after 5 min CO exposure at RT of Au/TiO_2, Ir/TiO_2 and $Ir\text{-}Au/TiO_2$ *in situ* reduced under H_2 at 400 °C. The introduction of CO on Au/TiO_2 leads to the appearance of a single carbonyl band at 2100 cm^{-1} attributed to CO adsorbed on low coordinated surface Au^0 atoms.[29,41,42] Monometallic Ir/TiO_2 presents an intense band with a maximum at 2064 cm^{-1} and a broad contribution in the low frequency side with two shoulders at 2032, 2000 and other weaker contributions at lower wavenumbers. The CO absorption bands in the 2065-2000 cm^{-1} region can be assigned to CO linearly adsorbed on different Ir^0 sites,[43–45] and the contributions at lower wavenumbers than 2000 cm^{-1} can be assigned to bridging CO adsorbed on two Ir^0 sites.[46] In the case of the $Ir\text{-}Au/TiO_2$ catalyst, the band at 2104 cm^{-1} assigned to CO adsorbed on Au^0 is visible. There is also a contribution in the same region as monometallic Ir/TiO_2 at 2051, 2032 and 2000 cm^{-1} but the component below 2000 cm^{-1} observed in the case of Ir/TiO_2 is not visible, which may indicate that the proportion of bridging CO species on Ir is smaller on $Ir\text{-}Au/TiO_2$. This could be an additional indication that bimetallic Ir-Au particles exists in $Ir\text{-}Au/TiO_2$, as alloying of iridium with gold would result in the disappearance of contiguous Ir sites. Moreover, the intensity of the bands of CO linearly adsorbed on Au^0 and Ir^0 are less intense than the ones observed for the monometallic counter-parts (Fig. 8A).

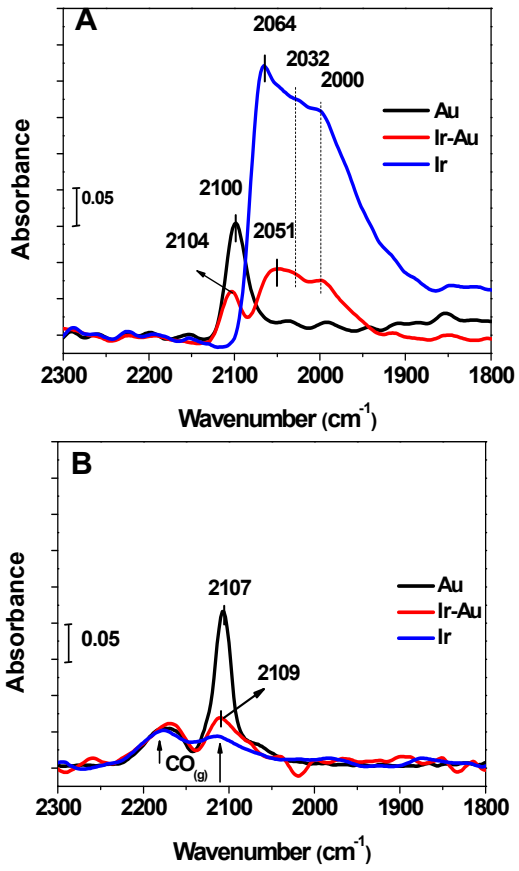

Fig. 8 DRIFT spectra after 5 min of CO adsorption on as-prepared Au/TiO_2, Ir/TiO_2 and $Ir\text{-}Au/TiO_2$ catalysts activated *in situ* at 400 °C under hydrogen (A) and under air (B).

This also suggests the existence of an interaction of both metals in the reduced Ir-Au catalyst.

DRIFTS experiments were also performed after *in situ* calcination at 400 °C. Fig. 8B compares the DRIFT spectra of calcined Au/TiO_2, Ir/TiO_2 and $Ir\text{-}Au/TiO_2$ after 5 min CO exposure at RT. The exposure of Au/TiO_2 to CO leads to the appearance of a band at 2107 cm^{-1} of CO linearly adsorbed on Au^0, as in the reduced sample. There is no visible band for Ir/TiO_2, which could be expected since Ir^{4+} species are not known to form stable carbonyls.[44,47–49] For the bimetallic $Ir\text{-}Au/TiO_2$ catalyst, only a very weak band at 2109 cm^{-1} assigned to CO on Au^0 is observed. The very low intensity of the band could be the result of interaction between the metallic gold and IrO_2 particles since the particles are smaller than those in Au/TiO_2 (Table 2).

4. Discussion

The various characterizations performed bring some information on the effect of combining Ir and Au in bimetallic samples. After reduction, according to the results of TPR (Fig. 2F) there is a limited reoxidation of the Ir species when gold and iridium are present in the same sample, indicating that gold

certainly interacts with iridium and stabilizes Ir against oxidation, at least to some extent as shown by XPS. Moreover, the shift in the position of the SPR band of the reduced Ir-Au sample (Fig. 3C) and the attenuation of its intensity, compared to that of the Au sample (Fig. 3A) also attest for interaction between gold and iridium in the particles. The results of CO-DRIFTS experiments on the reduced samples are also consistent with this interpretation (Fig. 8A), since even though there is the same amount of iridium in the mono and bimetallic samples, the intensity of the iridium contribution in the bimetallic Ir-Au/TiO_2 catalyst is much lower than the one in Ir/TiO_2 sample.

To the light of these characterizations, we can discuss the catalytic results that also demonstrate the influence of the conditions of thermal pretreatment at 400 °C, calcination or reduction, on the catalyst behavior in the reaction of propene oxidation. When the bimetallic Ir-Au/TiO_2 catalyst is calcined, the sample exhibits almost no activity below 250 °C (Fig. 4A); as mentioned above, calcination at 400 °C generates Au^0 and IrO_2 in the bimetallic sample, and their interaction attested by the DRIFTS results, does not improve the catalytic activity compared to the monometallic Au samples. This could indicate that IrO_2 in interaction with gold does not behave as a better support than TiO_2 for propene oxidation.

In contrast, activation under H_2 has a positive effect on the catalytic activity of monometallic Ir/TiO_2 and a much stronger one for bimetallic Ir-Au/TiO_2. This indicates that metallic iridium is an active species for this reaction. Moreover, as observed by TPR (Fig. 2D), XPS (Fig. 7 and Table 3) and DRIFTS (Fig. 8), reduction at 400 °C of Ir-Au/TiO_2 induces the formation of Au^0-Ir^0 bimetallic particles that lead to a higher catalytic activity than the reduced monometallic counterparts, Au/TiO_2 or Ir/TiO_2, indicating a synergetic effect due to the interaction between both metals (Fig. 4B).

The issue of the presence of the hump when both the reduced Ir-Au/TiO_2 and Ir/TiO_2 catalysts are submitted to the first reaction run (Fig. 4), and of its absence during the second run, must be discussed. Before the first reaction run, both Ir and Au are reduced in the metallic state according to TPR whereas before the second run, Ir is fully oxidized in Ir/TiO_2 and partially oxidized in Ir-Au/TiO_2, according to the XPS data (Table 3). Moreover after the hump observed during the first run (reaction stopped at 150 °C), Ir is extensively oxidized in Ir/TiO_2 and partially oxidized in Ir-Au/TiO_2 (Table 3). It is tentatively proposed that the hump results from the oxidation of the monometallic Ir particles present in both samples. Actually, according to a former study of some of us[13] mentioned in the introduction, all of the particles in the reduced Au-Ir/TiO_2 catalyst are not only bimetallic, and some of them are monometallic Ir particles, according to Rietveld refinement and micro-EDS analysis. Moreover these monometallic Ir particles fully reoxidized in the course of the propene oxidation reaction, could explain the vanishment of the hump in the second run of reaction. On the other hand, the iridium alloyed to gold in the bimetallic particles remains reduced as Ir^0-Au^0, which maintains the high activity in the second cycle reaction (Fig. 5A). This raises the question for Ir/TiO_2, why the reduced sample exhibits a higher activity ($T_{50\%}$ = 235 °C Fig. 5B) in the second reaction run than the calcined one ($T_{50\%}$ = 270 °C Fig. 4A) since in both cases Ir appears fully oxidized at the end of the first reaction run by XPS; this could be due to the formation of smaller IrO_2 particles during the reaction of propene oxidation than during calcination at 400 °C, because the Ir^0 particles that give rise to IrO_2 in the second reaction run are smaller (1.3 nm) than the particles formed by calcination (1.7 nm).

5. Conclusion

The present work shows that the addition of iridium to Au/TiO_2 catalyst does not lead to a better catalyst in propene oxidation when the catalyst is activated under air in spite of the evidence of interaction between Au^0 and IrO_2; this indicates that IrO_2 is not a better support for gold nanoparticles than titania for this reaction. In contrast, the activation under hydrogen leads to a much higher activity for Ir/TiO_2 than for Au/TiO_2, indicating that metallic iridium is an active species for propene oxidation. However, the stronger improvement of activity is observed for Ir-Au/TiO_2. The different characterizations allow assigning the high activity of Ir-Au/TiO_2 to a synergetic effect resulting from the formation of Ir-Au bimetallic particles. The characterizations also show that the presence of gold hinders the reoxidation of iridium in bimetallic sample at least to some extent when the sample is exposed to air and under reaction conditions of propene oxidation, which result in the preservation of the activity of the bimetallic catalyst during the second run of reaction.

Acknowledgements

The authors acknowledge financial support given by projects PAPIIT 103513 and CONACYT 130407. They also thank the French-Mexican program ECOS-ANUIES-SEP-CONACYT for funding the collaboration between Mexico and France. Antonio Aguilar-Tapia gratefully acknowledges CONACYT for this PhD Scholarship.

References

1 M. A. Centeno, M. Paulis, M. Montes and J. A. Odriozola, *Appl. Catal. A*, 2002, **234**, 65–78.
2 D. Andreeva, R. Nedyalkova and M. V. Abrashev, *Appl. Catal. A*, 2003, **246**, 29.
3 A. C. Gluhoi, S. D. Lin and B. E. Nieuwenhuys, *Catal. Today2*, 2004, **90**, 175.
4 A. Gluhoi, N. Bogdanchikova and B. Nieuwenhuys, *J. Catal.*, 2005, **232**, 96–101.
5 C. Della Pina, N. Dimitratos, E. Falleta, M. Rossi and A. Siani, *Gold Bull.*, 2007, **40**, 67.
6 M. I. Domínguez, M. Sánchez, M. A. Centeno, M. Montes and J. A. Odriozola, *J. Mol. Catal. A*, 2007, **277**, 145.
7 S. Y. Liu and S. M. Yang, *Appl. Catal. A*, 2008, **334**, 92.
8 L. Delannoy, K. Fajerwerg, P. Lakshmanan, C. Potvin, C. Méthivier and C. Louis, *Appl. Catal. B. Environ.*, 2010, **94**, 117–124.

9 M. Daté, M. Okumura, S. Tsubota and M. Haruta, *Angew. Chem. Int. Ed.*, 2004, **43**, 2129.
10 T. Akita, M. Okumura, K. Tanaka, S. Tsubota and M. Haruta, *J. Electron Microsc.*, 2003, **52**, 119–124.
11 Z. P. Liu, S. J. Jenkins and D. A. King, *Phys. Rev. Lett.*, 2004, **93**, 156102.
12 A. Gómez-Cortez, G. Díaz, R. Zanella, H. Ramírez, P. Santiago and J. M. Saniger, *J. Phys. Chem. C*, 2009, 9710–9720.
13 X. Bokhimi, R. Zanella and C. Angeles-Chavez, *J. Phys. Chem. C*, 2010, **114**, 14101–14109.
14 H. Hasen, *Constitution of Binary Alloys*, Mc Graw-Hill, New York, 1958.
15 G. C. Bond, *Gold Bull.*, 2001, **34**, 117.
16 S. Liu, Y. Cong, Y. Huang, X. Zhao and T. Zhang, *Catal. Today*, 2011, **175**, 264–270.
17 M. Okumura, N. Masuyama, E. Konishi, S. Ichikawa and T. Akita, *J. Catal.*, 2002, **208**, 485–489.
18 R. Zanella, L. Delannoy and C. Louis, *Appl. Catal. A*, 2005, **291**, 62–72.
19 R. Zanella, S. Giorgio, C. R. Henry and C. Louis, *J. Phys. Chem. B*, 2002, **106**, 7634–7642.
20 R. Zanella and C. Louis, *Catal. Today*, 2005, **107-108**, 768–777.
21 R. Zanella, S. Giorgio, C. R. Henry and C. Louis, *J. Phys. Chem. B*, 2002, 7634–7642.
22 A. Sandoval, A. Aguilar, C. Louis, A. Traverse and R. Zanella, *J. Catal.*, 2011, **281**, 40–49.
23 A. Gómez-Cortés, G. Díaz, R. Zanella, H. Ramírez, P. Santiago and J. M. Saniger, *J. Phys. Chem. C*, 2009, **113**, 9710–9720.
24 V. Idakiev, L. Ilieva, D. Andreeva, J. L. Blin, L. Gigot and B. L. Su, *Appl. Catal. A*, 2003, **243**, 25–39.
25 A. Sandoval, A. Gómez-Cortés, R. Zanella, G. Díaz and J. M. Saniger, *J. Mol. Catal. A*, 2007, **278**, 200–2008.
26 P. Reyes, D. Salinas, P. Campos, M. Oportus, J. Murcia, H. Rojas, G. Borda and J. L. G. Fierro, *Quim. Nov.*, 2010, **33**, 777–780.
27 J. A. Reyes-Esqueda, A. Bautista-Salvador and R. Zanella, *J. Nanosci. Nanotechnol.*, 2008, **8**, 3843–3850.
28 O. G. Morales-Saavedra and R. Zanella, *Mater. Chem. Physiscs*, 2010, **124**, 816–830.
29 A. Sandoval, C. Louis and R. Zanella, *Appl. Catal. B. Environ.*, 2013, **140-141**, 363–377.
30 S. Kundu and H. Liang, *J. Colloid Interface Sci.*, 2011, **354**, 597–606.
31 H. Baida and P. Diao, *Rare Met.*, 2012, **31**, 523–530.
32 R. Zanella, S. Giorgio, C. H. Shin, C. R. Henry and C. Louis, *J. Catal.*, 2004, **222**, 357–367.
33 Y. Lee, D. Kim, S. Shin and S. Oh, *Mater. Chem. Physiscs*, 2006, **100**, 85.
34 J. Sun, S. Fujita, F. Zhao, M. Hasegawa and M. Arai, *J. Catal.*, 2005, **230**, 398.
35 A. C. Gluhoi, X. Tang, P. Marginean and B. E. Nieuwenhuys, *Top. Catal*, 2006, **39**, 1.
36 P. Lakshmanan, L. Delannoy, V. Richard, C. Méthivier, C. Potvin and C. Louis, *Appl. Catal. B. Environ.*, 2010, **96**, 117–125.
37 L. Ilieva, G. Pantaleo, J. W. Sobczak, I. Ivanov, A. M. Venezia and D. Andreeva, *Appl. Catal. B. Environ.*, 2007, **76**.
38 P. Chen, J.-Q. Lu, G.-Q. Xie, G.-S. Hu, L. Zhu, L.-F. Luo, W.-X. Huang and M.-F. Luo, *Appl. Catal. A*, 2012, **433-434**, 236–242.
39 P. Reyes, H. Rojas and J. L. G. Fierro, *J. Mol. Catal. A*, 2003, **203**, 203–211.
40 A. Yoshida, Y. Mori, T. Ikeda, K. Azemoto and S. Naito, *Catal. Today*, 2013, **203**, 153–157.
41 F. Bocuzzi, A. Chiorno and M. Mazoli, *Surf. Sci.*, 2000, **454/456**, 942–946.
42 M. Daté, H. Imai, S. Tsubota and M. Haruta, *Catal. Today*, 2007, **122**, 222–225.
43 F. Solymosi and J. Rasko, *J. Catal.*, 1980, **62**, 253.
44 F. Solymosi, E. Novak and A. Molnar, *J. Phys. Chem.*, 1990, **94**, 7250.
45 Y. M. López-De Jesús, A. Vicente, G. Lafaye, P. Marecot and C. T. Williams, *J. Phys. Chem. C*, 2008, **112**, 13837–13845.
46 C. R. Guerra and J. H. Schulman, *Surf. Sci.*, 1967, **7**, 229–249.
47 I. Bukhardt, D. Gutschick, H. Landmesser and H. Miessner, in *Zeolite Chemistry and Catalysis*, ed. E. P.A. Jacobs, Elsevier, Amsterdam, 1991, p. 215.
48 P. Gelin, A. Auroux, Y. Ben Tarit and P. Gravelle, *Appl. Catal.*, 1989, **46**, 227.
49 K. I. Hadjiivanov and G. N. Vayssilov, *Adv. Catal.*, 2002, **47**, 307–511.

Supporting information

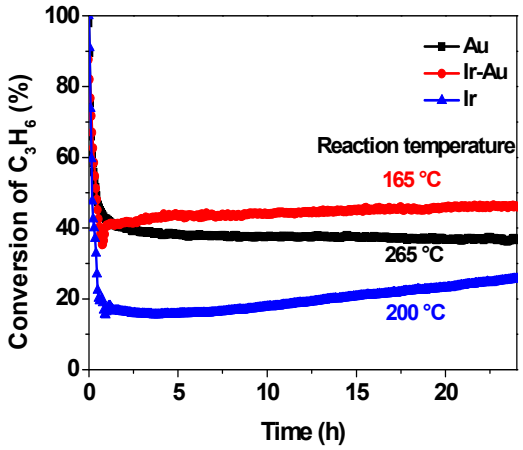

Fig. 1S Evolution of conversion of propene as a function of time on stream of reaction mixture over monometallic Au/TiO_2 (square) Ir/TiO_2 (triangle) and bimetallic $Ir\text{-}Au/TiO_2$ (circle) samples activated at 400 °C under H_2.